Geophysical Research Letters

RESEARCH LETTER
10.1029/2023GL106246

The Energy Decay of Warm-Core Eddies in the Gulf of Mexico

Thomas Meunier[1], Amy Bower[1], Paula Pérez-Brunius[2], Federico Graef[2], and Amala Mahadevan[1]

[1]Woods Hole Oceanographic Institution, Woods Hole, MA, USA, [2]CICESE, Ensenada, Mexico

Key Points:

- Time evolution of the energy of warm-core rings in the Gulf of Mexico is assessed using empirical methods and satellite altimetry
- The vast majority of mechanical energy (kinetic plus available potential) is lost early in the eddies' life cycles, far from the western boundary
- Wind-current feed back effects play an important role in energy conversion and decay

Correspondence to:

T. Meunier,
tmeunier@whoi.edu

Citation:

Meunier, T., Bower, A., Pérez-Brunius, P., Graef, F., & Mahadevan, A. (2024). The energy decay of warm-core eddies in the Gulf of Mexico. *Geophysical Research Letters*, *51*, e2023GL106246. https://doi.org/10.1029/2023GL106246

Received 13 SEP 2023
Accepted 7 NOV 2023

Author Contributions:

Conceptualization: Thomas Meunier
Data curation: Thomas Meunier
Formal analysis: Thomas Meunier, Amala Mahadevan
Funding acquisition: Amy Bower
Investigation: Thomas Meunier
Methodology: Thomas Meunier, Paula Pérez-Brunius
Project Administration: Amy Bower
Software: Thomas Meunier, Paula Pérez-Brunius
Validation: Thomas Meunier
Visualization: Thomas Meunier
Writing – original draft: Thomas Meunier
Writing – review & editing: Thomas Meunier, Amy Bower, Paula Pérez-Brunius, Federico Graef, Amala Mahadevan

Abstract The Gulf of Mexico (GoM) is home to some of the most energetic eddies in the ocean. Warm-core rings detach from the Loop-Current and drift through the basin, transporting large amounts of heat and salt. These eddies, known as Loop Current rings (LCRs) have a crucial role in the GoM's dynamics and in the weather of the eastern US, and this role is largely conditioned by their longevity and decay properties. Here, we use an empirical method to estimate the energy evolution of all LCRs detached since 1993. We found that, contrary to the commonly accepted idea that LCRs conserve their energy as they drift through the GoM and decay suddenly against the western platform, LCRs' energy decay is faster in the eastern basin, and they typically lose three-quarter of their energy before encountering the continental shelf. We also show that wind-current feedback contributes to the energy decay and conversion.

Plain Language Summary Ocean eddies can be long-lived and carry large amounts of heat and salt across ocean basins and marginal seas. This is the case of Loop Current rings (LCRs), which are large warm-core eddies drifting through the Gulf of Mexico (GoM). Understanding how these eddies lose their energy is key to understand their longevity and transport properties. Here, we use a previously validated empirical method based on in situ observations to estimate the time evolution of LCRs energy using satellite observations. We show that LCRs decay continuously during their life cycle, contrary to the previously accepted idea that they decay when collapsing against the western GoM's continental shelf. LCRs typically lose three-quarter of their energy before reaching any topographic obstacle. Using wind observations, we also show that wind-current interactions are key to the energy loss of these eddies.

1. Introduction

Coherent eddies can carry tracers across oceanic basins and participate in the transport of water-masses that impact large scale circulation and climate as well as ecosystems. For instance, Loop Current rings (LCRs), detaching from the Loop Current (LC), carry warm subtropical underwater (SUW) originating from the Caribbean through the Gulf of Mexico (Elliott, 1982; Leben, 2005) and have a direct impact on the basin's water mass properties (Hamilton et al., 2018; Meunier et al., 2020; Vidal et al., 1994), hurricane intensification (Jaimes et al., 2016; Shay et al., 2000), and thunderstorm occurrence east of the Rocky mountains (Molina et al., 2016). Similarly, Agulhas rings carry anomalously warm and salty Indian Ocean water through the South Atlantic and participate in the upper limb of the Atlantic Meridional Overturning Circulation (Beal et al., 2011; Biastoch et al., 2008; Marsh et al., 2007). The ability of such mesoscale eddies to be efficient in tracer transport, as well as the geographical characteristics of the heat, salt, or biogeochemical properties redistribution they induce, is directly controlled by their longevity and energy decay properties.

Although the processes responsible for the formation of LCRs have been (and remain) the focus of intense research (e.g., Candela et al., 2002; Donohue et al., 2016; Le Hénaff et al., 2023; Lugo-Fernández et al., 2016; Oey et al., 2003), the processes responsible for their decay have received less attention. As of now, the decay of LCRs has been largely attributed to two processes: vortex-splitting (Biggs et al., 1996; Forristall et al., 1992; Lipphardt et al., 2008) and topographic interactions along the western GoM's continental slope, which was consequently nicknamed the *eddy graveyard* (Biggs, 1992; Hamilton et al., 1999; Vidal et al., 1994). However, these studies were all mostly descriptive and limited to a small number of eddies, and did not provide large-number statistics on the decay of LCRs based on a relevant metric such as energy.

Using 25 years of satellite altimetry and an empirical relationship between sea surface height (SSH) and heat content, Meunier et al. (2020) showed that, on average, LCRs have already lost over two thirds of their heat content before they reach the so-called *eddy graveyard*, and that heat decays at an inverse exponential rate right

from the start of LCRs' life cycle, so that some other processes have to be invoked for the decay of LCR's heat content.

Beyond vortex-splitting and topographic effects, many processes can contribute to the decay of a mesoscale eddy. These include frontal instability (Brannigan et al., 2017; Pérez et al., 2022), interaction with submesoscale eddies (de Marez et al., 2020; Jouanno et al., 2016; Tedesco et al., 2019), mesoscale straining (Mariotti et al., 1994), layering and double diffusion (Armi et al., 1989; Meunier et al., 2015; Middleton et al., 2021; Schmitt et al., 1986), interaction with internal gravity waves (Joyce et al., 2013; Kunze, 1986; Polzin, 2008), surface heat fluxes (Dewar, 1987), or wind-current interactions (Dewar & Flierl, 1987; Duhaut & Straub, 2006; Renault, Molemaker, Gula, et al., 2016).

Of all these processes, wind-current interactions in the form of current feedback on the wind stress are of special interest, since the latter was shown numerically to yield a reduction of 20%–35% of eddy kinetic energy in eddying currents (Duhaut & Straub, 2006; Renault, Molemaker, Gula, et al., 2016; Renault et al., 2017). This process, based on the simple idea that wind stress depends on relative wind speed in a frame of reference moving with the current, rather than absolute wind speed, has consequences in the wind-stress distribution over a mesoscale eddy. The wind stress is increased where the current opposes the wind, and decreased where the current flows in the direction of the wind. This results in a systematic negative wind stress work integrated over an eddy's surface, which transfers kinetic energy (KE) from the ocean to the atmosphere (Dewar & Flierl, 1987), as well as Ekman pumping which induces a negative buoyancy flux that converts available potential energy (APE) into KE (Gaube et al., 2015; Wilder et al., 2022). While these processes were studied in depth in eddying current systems using regional numerical models (Renault, Molemaker, Gula, et al., 2016; Renault et al., 2017), their impact on individual mesoscale eddies remains largely unknown apart from the extremely idealized studies of Dewar and Flierl (1987) and Wilder et al. (2022), which suggest a significant impact of current-feed back on numerical, isolated, idealized eddies. The numerical study of Larrañaga et al. (2022) is of particular interest since it is focused on the LC system. They showed that including the current-feedback in their GoM regional model was associated with more realistic LCR shedding frequency, and even more interestingly, with a more accurate representation of LCR's longevity, suggesting that current-feedback exerts some control on the decay of LCRs. However, observational evidence of the impact of current-feedback on mesoscale eddies are still lacking.

Recently, Meunier et al. (2022) applied an empirical method known as the gravest empirical mode method (GEM) (Sun & Watts, 2001; Watts et al., 2001) to reconstruct the daily three-dimensional temperature and salinity structure of all LCRs detached in the GoM between 1993 and 2022. Their method was validated against in situ glider observations, and showed a striking accuracy (coefficient of determination R^2 greater than 0.93 between the GEM-reconstructed and the directly observed fields).

In this paper, we take advantage of this validated reconstruction method to estimate the energy decay properties, in time and space, of 40 LCRs detached between 1993 and 2023. Using scatterometer and reanalysis wind products, we also estimate the effect of wind-current feedback on the decay of the eddy's total energy and the conversion of its available potential energy to kinetic. Beyond a regional study of some particular class of eddy, to the best of our knowledge, this work is the first systematic observation-based statistical study of the energy decay of mesoscale eddies, as well as the first observation-based estimate of the relative impact of wind-current interactions on the decay and conversion of eddy energy. The results of this study could therefore provide some insight on the processes controlling mesoscale eddy decay in the ocean.

2. Data

This work is largely based on altimeter-derived sea surface height (SSH) observations. We use daily AVISO absolute dynamic topography (ADT) gridded fields. The grid has a 1/4° degree resolution and the data is available from 1 January 1993 until now.

As in Meunier et al. (2022), we also use nearly 7,000 Argo profiles distributed over the entire deep GoM (Figure 1a). Most of these floats were launched as part of the National Academies of Sciences Understanding Gulf Ocean Systems (UGOS) program.

The main wind product used is IFREMER CERSAT Global Blended Mean Wind Fields, which combines scatterometer observations with ECMWF operational wind analyses. The product is available on a 1/4° grid every 6 hr.

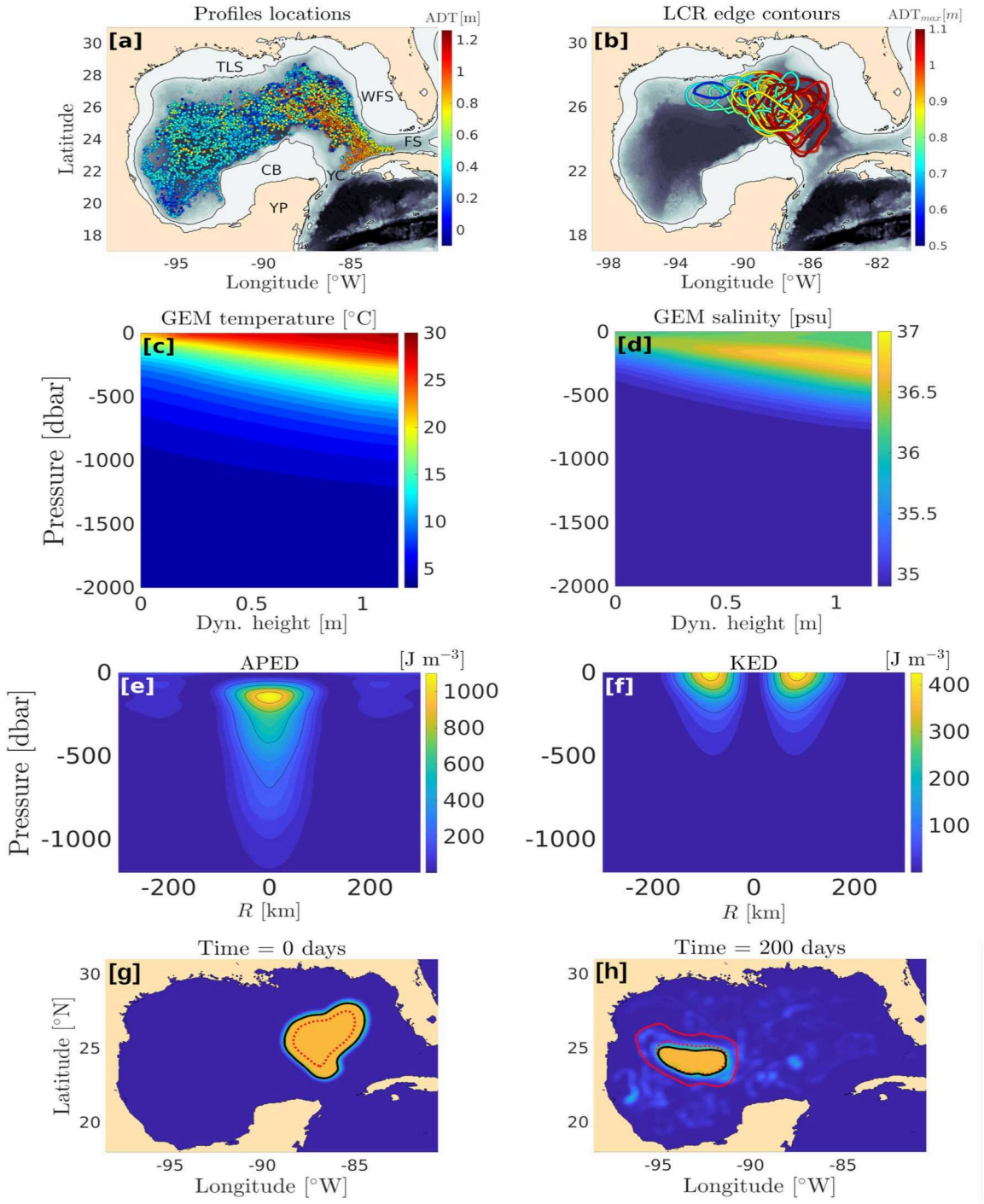

Figure 1. (a) Location of the profiles used to build the gravest empirical modes (GEM) for the Gulf of Mexico (GoM). The color represents the local altimetry (absolute dynamic topography; ADT). The names of the GoM's main topographic features are indicated. YC stands for Yucatan channel, FS stands for Florida strait, WFS stands for West Florida shelf, CB stands for Campeche bank, YP stands for Yucatan peninsula, and TLS stands for Texas-Louisiana shelf. (b) Edge contours on the first day after detachment for all Loop Current Rings (LCR) detached between 1993 and 2023. The color corresponds to the ADT value found in the center of the eddy, which often coincides with the maximum ADT value. (c) GEM transfer function for temperature. The *x*-axis is dynamic height, the *y*-axis is pressure, and the color map is temperature. (d) Same as (c) for salinity. (e) Available potential energy density section across an average LCR reconstructed using the GEM method. (f) Same as (e) for kinetic energy density. (g) Initial particle concentration in LCR Poseidon on detachment date. The dashed red line represents the maximum velocity contour. Normalized passive tracer concentration is color-coded (yellow is 1 and dark blue is zero). The concentration-based edge contour of Poseidon is materialized as a thick black line, and initially corresponds to the last closed contour. (h) Same as (g) after 200 days. The plain red line represents the last closed ADT contour.

A 24 hr averaging was performed to coincide with the ADT observations. Detailed information as well as a retrospective study of the product's performance can be found in Desbiolles et al. (2017). Scatterometers estimate the wind field by observing the sea-state. Since the latter depends on the wind relative to the current (not the absolute wind), scatterometer wind products are known to retain some signal of the current feedback (Plagge et al., 2012). Although this effect is attenuated by the gridding process, we compared the scatterometer product's results with data from ECMWF's ERA5 reanalysis, which provides estimates of the absolute wind. ERA5 is based on a 4DVAR ensemble data assimilating atmospheric model and is distributed as hourly outputs on a 1/4° grid. Here, a 24 hr averaging was also performed. Full details about the methods can be found in Hersbach et al. (2020).

For both wind products, wind stress was computed using the COARE3.5 parameterization (Edson et al., 2013).

3. Methods

3.1. Theoretical Background

In this study, we seek to describe the time evolution of the total mechanical energy (hereafter total energy; TE) of individual eddies, which is the three-dimensional integral of energy density over the eddy's volume.

The evolution equation for kinetic energy density $\left(E_k = \frac{1}{2}\rho|\mathbf{u}|^2\right)$ reads (Gill, 1982):

$$\frac{DE_k}{Dt} + \rho' g w = -\nabla \cdot P'\mathbf{u} + \mathbf{u} \cdot \frac{\partial \boldsymbol{\tau}}{\partial z} + \nabla \cdot \mathrm{K}\nabla E_k + \rho\epsilon, \tag{1}$$

where E_k is kinetic energy density, $\frac{D}{Dt}$ is the material derivative, ρ' is density anomaly referenced to a minimum potential energy profile, w is vertical velocity, P' is pressure anomaly, $\mathbf{u}$ is the velocity vector, $\boldsymbol{\tau}$ is the stress, z is the vertical coordinate, $\mathbf{K}$ is a diagonal diffusivity coefficient tensor and ϵ is the energy dissipation rate. The minimum potential energy profile is built by adiabatically sorting all available Argo profiles from the Gulf of Mexico, following the classical methods of Winters et al. (1995).

The second term on the left-hand side is the buoyancy flux, and is equal to the material rate of change of APE density (Holliday & McIntyre, 1981):

$$\frac{DE_p}{Dt} = \rho' g w, \tag{2}$$

so that the left-hand side of Equation 1 represents the material rate of change of total energy density ($E_t = E_k + E_p$). Following Holliday and McIntyre (1981), APE density is defined as:

$$E_p = -\int_0^{\eta} g\tilde{\eta}\left.\frac{\partial \rho_r}{\partial z}\right|_{z-\tilde{\eta}} d\tilde{\eta}, \tag{3}$$

where ρ_r is the reference potential density profile (with minimum potential energy) and η is the isopycnal displacement, relative to the reference profile. In this work, we study the effects of the (relative) wind on energy decay and energy conversion, and we compute the buoyancy flux of Equation 2 using the non-linear Ekman pumping vertical velocity (Stern, 1965):

$$w_e = \frac{1}{\rho_0}\nabla \times \left(\frac{\boldsymbol{\tau}}{f+\zeta}\right) \tag{4}$$

Note that computing the non-forced vertical velocity using the Omega equation was also considered, but, since the estimated fields are not necessarily solutions of any equation of motion, and given the relatively low spatial resolution, the omega-derived vertical velocity is essentially noise, with zero-mean vertical velocity. Note also that relative vorticity is small compared to the Coriolis frequency (Rossby numbers of ≈[0.05–0.15]), so that the bottom term is dominated by the planetary vorticity.

As mentioned above, the wind stress to be considered here is the relative wind stress, which takes into account the feedback of the current and reads:

$$\boldsymbol{\tau} = \rho_a C_d |\boldsymbol{u_a} - \alpha \boldsymbol{u_g}|\left(\boldsymbol{u_a} - \alpha \boldsymbol{u_g}\right), \tag{5}$$

where ρ_a is air density, C_d is the drag coefficient computed using the COARE3.5 parameterization (Edson et al., 2013), $\boldsymbol{u_a}$ is the absolute wind velocity 10 m above the sea surface and $\boldsymbol{u_g}$ is the velocity of the surface current, computed from the altimetry-derived SSH using the geostrophic balance assumption. α is a coefficient applied to the current velocity to account for the feedback of the stress increase/reduction by the current-feedback through frictional effects, that results in a reduction/increase of the absolute wind speed (Renault, Molemaker, McWilliams, et al., 2016). We used values of 1 and 0.7 for α, following empirical results of Renault et al. (2019).

We are interested in quantifying the evolution of the total energy ($\mathbb{E}_\mathbf{t}$) transported by an eddy whose boundary is defined by the closed line C which encircles the surface S:

$$\mathbb{E}_\mathbf{t} = \iint_S \int_{-H}^{0} E_t \, dz \, ds, \tag{6}$$

where ds is a surface element and H is the eddy's thickness (the depth below which density anomaly is zero). We do not make the hypothesis that the boundary C is a material line. Integrating the left hand side of Equation 1 in its flux form, using the Ostrogradski theorem, the Leibniz theorem, and the Reynolds transport theorem, we get an exact equation for the evolution of total energy, under the assumption that the thickness does not vary:

$$\frac{d}{dt}\mathbb{E}_\mathbf{t} = \int_{-H}^{0} \Bigg\{ \overbrace{\oint_C (\mathbf{u_c} - \mathbf{u}) \cdot \mathbf{n} E_t \; dl}^{(a)} - \overbrace{\oint_C \mathbf{u} \cdot \mathbf{n} P' \; dl}^{(b)} + \overbrace{\iint_S \mathbf{u} \cdot \frac{\partial \tau}{\partial z} ds}^{(c)} + \underbrace{\oint_C \mathbf{K} \nabla E_k \cdot \mathbf{n} \; dl}_{(d)} + \underbrace{\iint_S \rho \epsilon \; ds}_{(e)} \Bigg\} dz \tag{7}$$

The first term on the right hand side represents the energy flux through the eddy's boundary that is caused by the relative flow in the eddy's moving referential. In the case of a Lagrangian coherent vortex, the boundary C is a material line, so that it is exactly advected by the flow ($\mathbf{u_c} = \mathbf{u}$) and the term vanishes. The second term is the work of the pressure force. Under the geostrophic approximation, it is null whatever the boundary. The third term is the wind stress work. Since the wind stress is dependent on the relative wind speed, even an homogeneous wind will exert some work, whose integral over the eddy's surface will be negative, whatever the vorticity sign (Dewar & Flierl, 1987). The viscous terms (d) represent all the unresolved (sub-grid scale) advective turbulent processes that might cause an energy flux through the eddy's boundary (which is only defined using coarse resolution observations) and the dissipation term (e) is essentially related to small scale turbulence yielding conversion of mechanical energy to internal energy.

Because we are interested in examining and comparing the energy evolution of a set of eddies of different sizes, we need to use a normalized metric. The surface-averaged energy is a convenient variable:

$$\overline{E}_t = \frac{\mathbb{E}_\mathbf{t}}{S}, \tag{8}$$

where S is the total surface of the eddy $\left(S = \iint_S ds\right)$. Integrating Equation 7 with respect to time and dividing by the instantaneous area of the eddy, we get an equation for the surface-averaged energy density.

$$\overline{E}_t(t) = \frac{1}{S} \int_0^t \int_{-H}^{0} \{(a) + (b) + (c) + (d) + (e)\} dz \; d\tilde{t} \tag{9}$$

Since our purpose is to compute statistical properties of energy decay by ensemble-averaging over all the detached eddies, using the surface-averaged energy density is convenient. Ensemble averaging using the integrated total energy would introduce a bias by increasing the weight of large eddies in the average. Normalizing total energy

by each eddy's area avoids this bias. More interestingly, normalizing energy by the eddy's area also removes the effects of energy loss due to direct loss or gain of area (hence mass), as can happen during filamentation or splitting/merging events. For the sake of concision, in the rest of the paper, the terms KE, APE and TE will be used to designate the surface averaged kinetic, available potential and total energy density. When studying the impact of the current-modified wind stress on the eddies' energy, the two variables we will focus on are the surface-averaged, time-integrated wind stress work, normalized by the TE's initial value of each eddy that we will casually refer to as the wind stress work (WSW), and the surface-averaged, time-integrated Ekman pumping buoyancy flux, normalized by the initial value of APE of each eddy, that we will casually refer to as the Ekman pumping buoyancy flux (EPBF):

$$\mathrm{WSW}(t) = \frac{1}{\overline{E}_t(0)} \frac{\int_0^t \iint_S \boldsymbol{\tau}(\tilde{t}) \cdot \boldsymbol{u_g}(\tilde{t}) ds d\tilde{t}}{S(t)}, \tag{10}$$

$$\mathrm{EPBF}(t) = \frac{1}{\overline{E}_p(0)} \frac{\int_0^t \int_{-H}^0 \iint_S \rho' g w_e ds \; dz \; d\tilde{t}}{S(t)}. \tag{11}$$

3.2. The Gravest Empirical Mode Method (GEM)

To estimate the daily 3D structure of temperature and salinity (hence geostrophic velocity, KE and APE density) from satellite altimetry, we use an empirical method known as the gravest empirical mode projection (GEM) (Meunier et al., 2022; Sun & Watts, 2001; Watts et al., 2001). It consists of establishing an empirical relationship between the vertical thermohaline structure of the ocean and the dynamic height to build transfer functions that associate one single value of temperature and salinity for each pair {pressure, SSH}. The procedure used here was used and validated in the Gulf of Mexico and is described in details in Meunier et al. (2022). The mean yearly transfer functions for salinity and temperature are shown in Figures 1c and 1d, respectively: the downward sloping of the isotherms and of the subsurface salinity maximum with increasing SSH, associated with the subtropical underwater (SUW) carried by LCRs is evident. Note that, to account for the seasonality of surface conditions, which affects the accuracy of the three-dimensional reconstruction in the top 200 dbar, the GEM fields were constructed on a monthly basis. KE is computed using the geostrophic velocity, assuming no motion at 2000 dbar. An example of APE and KE density cross-section reconstructed using the GEM along with an average LCR's SSH anomaly is shown in Figures 1e and 1f, respectively. APE is concentrated in the core of the eddy, while KE is stronger near the edges, where density gradients are sharper. The APE maximum is 2.5 times larger than the KE maximum and, when integrated over the whole LCR, APE largely dominates over KE (Meunier et al., 2022).

3.3. Eddies' Edge Definition

In this work, we aim to follow the whole LCR, and not only its coherent part, which is usually confined to a small portion of the core (Andrade-Canto et al., 2020; Beron-Vera et al., 2018). Hence, rather than tracking so called Lagrangian coherent vortices (Beron-Vera et al., 2013; Haller & Beron-Vera, 2013), the eddy as we wish to track it should be defined as a compact rotating body of water detached from the LC, regardless of its a priori conservation properties. The detection and tracking method is based on ADT. First we define the LC's edge as the smallest-value ADT contour linking the Yucatan channel and the Florida strait. This contour usually encloses closed ADT contours, which are the signature of unborn LCRs. We define LCR detachment as the instant at which none of the closed contours remain enclosed within the LC anymore. Once detached, to define the LCR's boundary, we use a mixed Eulerian-Lagrangian procedure: at $t = 0$ (detachment date), we initialize a cluster of virtual Lagrangian particles within the outermost closed SSH contour, which coincides with the boundary of the water mass detached from the LC. These particles are distributed on a 1 km × 1 km regular grid. They are then advected in the geostrophic surface velocity field inferred from the altimetry product, using a fourth-order Runge-Kutta scheme (Butcher, 1996). The particle concentration is then computed and interpolated on a regular 1/48° grid. The LCR's edge is defined as the concentration contour with the original value at $t = 0$, that is, the closed isopleth that encloses a compact surface of constant concentration equal to the original concentration. A sequence of particle concentration maps during the drift of LCR Poseidon in April and November 2016 is

shown on Figures 1g and 1h. The edge contour based on the concentration criterion is compared to two other Eulerian criteria: the Maximum velocity contour and the last closed SSH contour. While particle loss through filamentation of the eddy is evident, concentration within the eddy's boundary remain largely homogeneous. It is important to note that, while the method is based on Lagrangian particles integration, it does not belong to the class of *Lagrangian methods*, that seek coherent eddy boundaries, such as the null geodesics rings of Haller and Beron-Vera (2013) and Beron-Vera et al. (2018). Here, the boundary does not ensure the coherence of the eddy, in the sense that tracer conservation is not guaranteed (and our detected eddies actually do loose tracer). However, contrary to Lagrangian Coherent Vortices detected using proper *Lagrangian methods*, this method allows us to follow the entire body of water detached from the LC, and not only a small fragment of it. The initial boundaries of all eddies are shown in Figure 1b, where the SSH at the eddies' centers is color-coded.

4. Results

Individual trajectories of the 40 LCRs are shown on Figure 2a. TE, normalized by the initial values at the time of detachment, is color-coded. While a few LCRs maintain high levels of energy (>80%) past the Campeche bank, west of 93°W, the vast majority start losing energy sooner in their life cycle in the eastern GoM. The ensemble average of normalized TE for all LCRs is shown in Figure 2b. The circles' size represents the average diameter of LCRs during their drift. After 200 days, the average TE left in the eddies is only 26% of the initial value at detachment. This value is of 21% and 28% for KE and APE, respectively (not shown).

The evolution of the mean KE, APE and TE (non-normalized by initial values) is shown against time and longitude on Figure 2c. The 95% confidence interval, computed using the bootstrap method, is shown as the light shaded areas. APE largely dominates over KE during the entire eddies' life cycle. On average, both KE and APE start decaying right from the first days after detachment and keep on decaying continuously with time until 200 days, resulting in a similar decay of TE. The average halving time for KE, APE and TE is of 101 days, 120 days, and 117 days, respectively. Looking at the longitude-dependence of energy, a similar pattern appears: APE and KE start decaying in the eastern basin near 88.5°W and decay continuously across the entire GoM. The halving longitude is of 91°W for KE and 91.6°W for APE and TE. The energy decay rates (Figure 2d) not only confirm that energy loss occurs all along the eddies' drift through the GoM, but also that LCRs lose APE (and TE) at a faster rate in the eastern GoM, during the first month of their life cycle. KE does not exhibit this increased decay rate in the eastern basin, and decays at a constant rate all along the eddies life cycle.

Since previous works have pointed out some critical longitude (≈92–93°W) where eddies seem to decay at a faster rate, mostly because of instability and eddy-splitting (direct loss of mass; see Lipphardt et al. (2008) and references therein), we also investigated the evolution of the total LCRs energy (the energy density integrated over the full eddy's surface and not the energy per unit area discussed above) as well as the evolution of the eddies area, which would clearly indicate regions of more frequent splitting. The surface integrated KE, APE and TE, normalized by their initial values and ensemble-averaged are shown against time and longitude in Figures 2e and 2f, respectively. As for the surface-averaged KE, TE and APE, the surface integrated KE, TE and APE smoothly and regularly decay with time during the whole LCRs life cycle. Similarly, the decay against longitude shows no obvious rapid change, except for a slightly faster decay between 90 and 91°W. The evolution of the ensemble-averaged LCRs areas against time and longitude shows the same regular decay, without any evident sudden change.

Equation 7 shows that for a mesoscale geostrophic eddy, where the work of the pressure force is negligible, TE can only decay through the action of wind stress work, an energy flux through the boundary, and diffusivity. As mentioned above, the energy flux through the boundary is impossible to estimate, since the boundary's velocity is undefinable (because it is not defined by a series of material points, or material line), and the diffusive terms cannot be estimated with satellite altimetry and Argo data only. On the other hand, the effects of wind stress work can be assessed using wind observations. Similarly, the decay of APE is directly linked to buoyancy fluxes (Equation 3), and while the vertical velocity cannot be fully estimated, we still can estimate the contribution of Ekman pumping (Equation 4). In other words, while this work does not allow for a full budget of the energy equation, the effects of relative wind stress can be assessed. Figure 2g compares the average evolution of TE (normalized by initial values) to the effect of wind stress work for 4 different wind stress parametrization: absolute wind stress obtained from scatterometer products (SCAT abs), relative wind stress obtained from scatterometer products and computed by removing the full current velocity from the absolute wind value (SCAT rel), relative wind stress

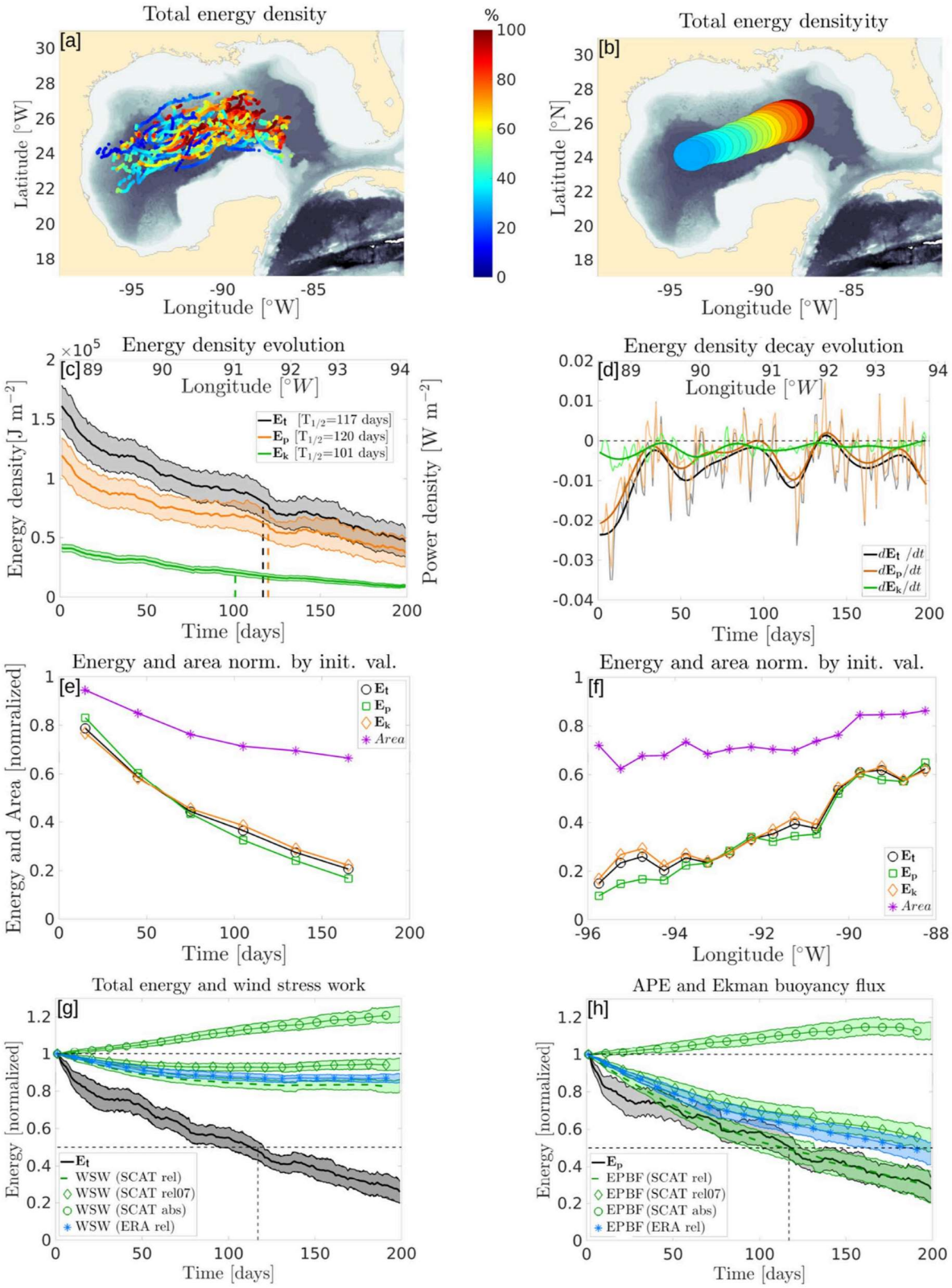

Figure 2.

obtained from the ERA5 reanalysis and computed by removing the full current velocity from the absolute wind value (ERA rel), and relative wind stress obtained from scatterometer products and computed by removing 70% of the current velocity to the absolute wind value (SCAT rel07). Relative wind stress work appears to contribute to the decay of the LCRs' TE, with an average of 18% and 15% of the original TE extracted when using Scatterometer and ERA5 wind products, respectively. This corresponds to respectively a quarter and a fifth of the energy lost by LCRs in 200 days. When using Renault et al. (2019)'s parameterization which uses a current velocity reduced by 30% to compute relative wind stress (SCAT rel07), we find that, on average, wind stress work only accounts for about 10% of the TE loss in LCRs. In all three cases, energy decay through wind stress work is faster in the beginning of the LCR's life cycle, and after about 120 days, wind stress work does not extract energy any more. For comparison, the work of the absolute wind was also computed. Surprisingly, it represents an energy source for LCRs with an average increase of the original TE by about 20% after 200 days. This shows that the mean spatial distribution of absolute wind in the GoM tends to increase the LCRs energy, showing that the energy sink is really related to wind-current interactions.

Time evolution of APE is compared to the effects of Ekman pumping buoyancy fluxes in Figure 2h. The wind parameterizations shown are the same as for Figure 2g. The close coincidence of the decay of APE and that expected from Ekman pumping buoyancy fluxes computed from scatterometer-derived relative wind stress is striking. It suggests that Ekman pumping buoyancy fluxes might account for the whole observed APE decay. Using ERA5 relative wind stress, we find that Ekman pumping buoyancy flux accounts for a slightly reduced part of the APE decay (70% of the APE loss after 200 days), and using the reduced current parameterization for relative wind stress computation (SCAT abs07), Ekman pumping buoyancy flux accounts for about 65% of the total APE loss in 200 days. Using absolute wind stress, we find that Ekman pumping buoyancy flux corresponds to an APE increase of nearly 20% during the first 170 days, followed by a small decrease in the last 30 days. The modest impact of absolute wind stress work, and the close resemblance of the results when using scatterometer and ERA5 wind products suggest that, once gridded, scatterometer-based wind fields retain little signal of the current-feed back and can be considered as a good proxy of the absolute wind.

5. Discussion and Conclusion

Using an observation-based method, we assessed the statistical properties of the energy decay of all LCRs detached since 1993. To the best of our knowledge, this is the first time such statistics on the energy decay of mesoscale eddies are obtained anywhere in the world ocean based on observations.

We showed that LCRs' energy decay is a fast process occurring continuously during the eddies' life cycles. This observation is in contradiction with the commonly accepted idea that LCRs steadily drift through the GoM, retaining their hydrographic properties until they collapse against the western platform, as explicitly shown in the numerical simulations of Romanou et al. (2004), and suggested in a number of other numerical studies listed in Lipphardt et al. (2008) (Dietrich et al., 1997; Kantha et al., 2005; Sturges et al., 1993). It should be pointed out that our results do not contradict the idea of an *eddy graveyard*, but clearly show that the decay of LCRs does not happen only there. The decay starts right from the first month after detachment from the LC and continues all along their life cycle. As they reach the so-called graveyard, LCRs are already old and weak eddies that have typically lost over 3/4 of their energy. Topographic effects in the western basin can therefore not be considered a major cause of LCR decay, but rather the ultimate process dispersing their remnants. Moreover, the energy decay rate was shown to be faster in the eastern basin soon after detachment than in the western basin, and the halving longitude is found as far East as 91.5°W.

Figure 2. (a) Trajectories of the centers of the 40 Loop Current Rings (LCR). Total energy normalized by its initial value is color-coded. (b) Ensemble-averaged TE normalized by its initial value. The position and diameter of the circles represent the average position and size of the LCRs. (c) Time evolution of the average energy density. The black, orange and green lines represent total energy (TE), available potential energy (APE), and kinetic energy (KE), respectively. The shaded areas around the lines represent the 95% confidence interval. The vertical dashed lines represent the energy halving time. The average longitude corresponding to the time is indicated on the top *x*-axis. (d) Time evolution of the ensemble averaged rate of change of energy density (time derivative of energy density). The dark thick lines represent the 30-days low pass filtered values, while the thin light lines represent the raw results. The color code is the same as in panel (c). (e) Ensemble average of the non-surface-averaged KE (orange diamonds), TE (black circles) and APE (green squares) and eddy's area (purple stars) normalized by their initial values against time. (f) Same as (e) against longitude. (g) Energy extraction by the effects of wind stress work. The dashed line represents wind stress work computed from the scatterometer data. The green diamonds represent wind stress work computed by reducing the current by a factor of a 0.7 when computing relative wind. The red circles represent the effect of wind stress work computed using the absolute wind stress. The blue stars represent the effect of wind stress work computed using the ERA5 reanalysis. Time evolution of the TE is indicated as a black line. (h) Energy conversion by the effect of the Ekman pumping buoyancy flux. The Color code is the same as in panel (g). Time evolution of APE is indicated as the black line.

Our results also contradict another long-standing claim that there exists some critical longitude in the GoM, between 92 and 93°W, beyond which LCRs suddenly decay at a fast rate, mostly through low wavenumber instability (the observed elliptization of the eddies seems consistent with the development of an azimuthal mode 2 vortex Rossby wave) yielding vortex-splitting (Hamilton et al., 1999; Lipphardt et al., 2008; Vukovich, 2007). Although we acknowledge that LCRs might become unstable, loose coherence or split as directly observed by Biggs et al. (1996) so that the decay rate might occasionally increase in the central basin, our results show no sign of a critical longitude between 92 and 93°W (nor anywhere) where LCRs loose mass or energy at a faster rate. The decay of the eddies' area and surface-integrated KE, APE and TE is a gradual process occurring all through their life cycles.

Beyond the description of the decay of energy in LCRs, we also investigated the possible role of wind-current feedback on that decay. We showed that the effect of relative wind stress work is non-negligible, but likely not a leading order mechanism in the decay of kinetic energy (and total energy) as it accounts for 25% and 20% of the total energy loss in 200 days when using scatterometer and ERA5 wind fields, respectively. When using Renault et al. (2019)'s parameterization to account for the diminution of absolute wind when the current opposes the wind (and vice versa) (by reducing the current velocity by 30% when computing relative wind stress), we found that wind stress work then only accounts for 10% of the total energy loss in 200 days.

However, the impact of current-feedback was shown to be important for the decay of APE, which would be entirely driven by Ekman pumping buoyancy flux when using relative wind stress computed from scatterometer data. Beyond this striking result, the control of APE loss by Ekman pumping buoyancy flux has implications on the decay of KE. Buoyancy flux does not extract TE: it converts APE to KE (it is often referred to as the baroclinic conversion term), which means that all along the LCRs life cycle, KE is fueled by this conversion. Given the modest role of wind stress work, this means that some other processes, such as turbulent diffusivity at the edges of the eddies (subgrid-scale advective processes that are unresolved by the altimetry grid) might be important in the decay of LCRs' TE through the decay of KE.

Of course, our study does not allow estimation of the impact of direct energy flux through the eddies' boundary which is related to the fact that the edges we consider are not material lines (term (a) in Equation 7). This is clearly a caveat of not using Lagrangian coherent boundaries, which would ensure the flux term to be zero, and would allow us to estimate the diffusive term as it would become the only unknown of Equation 7. The choice not to use such Lagrangian metrics was motivated by the need to estimate the evolution of the full detached patch of LC water, and not only a small piece of its core. In particular, relative wind stress work becomes important near the edge of the eddies, where the velocity is maximum, while long-horizon coherent LCRs usually exclude this peripheral part. However, working with three-dimensional Lagrangian objective eddy framing (Beron-Vera et al., 2013; Haller & Beron-Vera, 2013) would be complementary to this study. Although it would only allow to estimate the properties and fate of the inner core of LCRs, it could allow us to explore more accurately the impact of Ekman pumping buoyancy fluxes in baroclinic conversion.

Note that, while this study is focused on the GoM, similar processes are expected to occur in other warm-core rings (e.g., Agulhas rings, Gulf stream rings, Mozambic channel rings, North Brazil Current rings, Kuroshio rings etc.).

Data Availability Statement

All data used in this study are publicly available. Gridded scatterometer wind products (Scatterometer Wind Fields, 2023) were used to compute wind stress. Absolute dynamic topography SSH product (Absolute Dynamic Topography, 2023) was used to identify and reconstruct LCRs'structure as well as to compute geostrophic surface velocity. Data is available after users create a Copernicus account. The GEM were built using Argo float profiles (Argo, 2023). Argo data are available from any data assembly center specifying the geographical limits of [−99 −80]°W and [17 31]°N.

Acknowledgments
The authors are grateful to Mike Spall, Lionel Renault and Xavier Carton for their useful suggestions and comments. This work is part of the LC-floats and UGOS3 projects, funded by the US National Academy of Sciences through the Understanding Gulf Ocean Systems Grants 2000010488 and 200013145.

References

Absolute Dynamic Topography (2023). Global ocean gridded l 4 sea surface heights and derived variables reprocessed 1993 ongoing [ADT dataset]. Copernicus. https://doi.org/10.48670/moi-00148

Andrade-Canto, F., Karrasch, D., & Beron-Vera, F. J. (2020). Genesis, evolution, and apocalypse of Loop Current rings. *Physics of Fluids*, *32*(11), 116603. https://doi.org/10.1063/5.0030094

Argo (2023). Argo float data and metadata from Global Data Assembly Centre (Argo GDAC) [Argo dataset]. SEANOE. https://doi.org/10.17882/42182

Armi, L., Hebert, D., Oakey, N., Price, J. F., Richardson, P. L., Thomas Rossby, H., & Ruddick, B. (1989). Two years in the life of a mediterranean salt lens. *Journal of Physical Oceanography*, *19*(3), 354–370. https://doi.org/10.1175/1520-0485(1989)019⟨0354:TYITLO⟩2.0.CO;2

Beal, L. R., De Ruijter, W. R. R., Biastoch, A., Zahn, R., Cronin, M., Hermes, J., et al. (2011). On the role of the Agulhas system in ocean circulation and climate. *Nature*, *472*(7344), 429–436. https://doi.org/10.1038/nature09983

Beron-Vera, F. J., Olascoaga, M. J., Wang, Y., Triñanes, J., & Pérez-Brunius, P. (2018). Enduring Lagrangian coherence of a Loop Current ring assessed using independent observations. *Scientific Reports*, *8*(1), 11275. https://doi.org/10.1038/s41598-018-29582-5

Beron-Vera, F. J., Wang, Y., Olascoaga, M. J., Goni, G. J., & Haller, G. (2013). Objective detection of oceanic eddies and the Agulhas leakage. *Journal of Physical Oceanography*, *43*(7), 1426–1438. https://doi.org/10.1175/JPO-D-12-0171.1

Biastoch, A., Böning, C. W., & Lutjeharms, J. R. E. (2008). Agulhas leakage dynamics affects decadal variability in Atlantic overturning circulation. *Nature*, *456*(7221), 489–492. https://doi.org/10.1038/nature07426

Biggs, D. C. (1992). Nutrients, plankton, and productivity in a warm-core ring in the western. *Gulf of Mexico*, *97*(C2), 2143–2154. https://doi.org/10.1029/90JC02020

Biggs, D. C., Fargion, G. S., Hamilton, P., & Leben, R. R. (1996). Cleavage of a Gulf of Mexico Loop Current eddy by a deep water cyclone. *Journal of Geophysical Research*, *101*(C9), 20629–20642. https://doi.org/10.1029/96JC01078

Brannigan, L., Marshall, D. P., Naveira Garabato, A. C., Nurser, A. J. G., & Kaiser, J. (2017). Submesoscale instabilities in mesoscale eddies. *Journal of Physical Oceanography*, *47*(12), 3061–3085. https://doi.org/10.1175/JPO-D-16-0178.1

Butcher, J. C. (1996). A history of Runge-Kutta methods. *Applied Numerical Mathematics*, *20*(3), 247–260. https://doi.org/10.1016/0168-9274(95)00108-5

Candela, J., Sheinbaum, J., Ochoa, J., Badan, A., & Leben, R. (2002). The potential vorticity flux through the Yucatan channel and the Loop Current in the Gulf of Mexico. *Geophysical Research Letters*, *29*(22), 2059. https://doi.org/10.1029/2002GL015587

de Marez, C., Meunier, T., Morvan, M., L'Hégaret, P., & Carton, X. (2020). Study of the stability of a large realistic cyclonic eddy. *Ocean Modelling*, *146*, 101540. https://doi.org/10.1016/j.ocemod.2019.101540

Desbiolles, F., Bentamy, A., Blanke, B., Roy, C., Mestas-Nuñez, A. M., Grodsky, S. A., et al. (2017). Two decades [1992-2012] of surface wind analyses based on satellite scatterometer observations. *Journal of Marine Systems*, *168*, 38–56. https://doi.org/10.1016/j.jmarsys.2017.01.003

Dewar, W. K. (1987). Ventilating warm rings: Theory and energetics. *Journal of Physical Oceanography*, *17*(12), 2219–2231. https://doi.org/10.1175/1520-0485(1987)017⟨2219:VWRTAE⟩2.0.CO;2

Dewar, W. K., & Flierl, G. R. (1987). Some effects of the wind on rings. *Journal of Physical Oceanography*, *17*(10), 1653–1667. https://doi.org/10.1175/1520-0485(1987)017⟨1653:SEOTWO⟩2.0.CO;2

Dietrich, D. E., Lin, C. A., Mestas-Nunez, A., & Ko, D. S. (1997). A high resolution numerical study of Gulf of Mexico fronts and eddies. *Meteorology and Atmospheric Physics*, *64*(3–4), 187–201. https://doi.org/10.1007/BF01029692

Donohue, K. A., Watts, D. R., Hamilton, P., Leben, R., & Kennelly, M. (2016). Loop Current Eddy formation and baroclinic instability. *Dynamics of Atmospheres and Oceans*, *76*, 195–216. https://doi.org/10.1016/j.dynatmoce.2016.01.004

Duhaut, T. H. A., & Straub, D. N. (2006). Wind stress dependence on ocean surface velocity: Implications for mechanical energy input to ocean circulation. *Journal of Physical Oceanography*, *36*(2), 202–211. https://doi.org/10.1175/JPO2842.1

Edson, J. B., Jampana, V., Weller, R. A., Bigorre, S. P., Plueddemann, A. J., Fairall, C. W., et al. (2013). On the exchange of momentum over the open ocean. *Journal of Physical Oceanography*, *43*(8), 1589–1610. https://doi.org/10.1175/JPO-D-12-0173.1

Elliott, B. A. (1982). Anticyclonic rings in the Gulf of Mexico. *Journal of Physical Oceanography*, *12*(11), 1292–1309. https://doi.org/10.1175/1520-0485(1982)012⟨1292:ARITGO⟩2.0.CO;2

Forristall, G. Z., Schaudt, K. J., & Cooper, C. K. (1992). Evolution and kinematics of a loop current eddy in the Gulf of Mexico during 1985. *Journal of Geophysical Research*, *97*(C2), 2173–2184. https://doi.org/10.1029/91JC02905

Gaube, P., Chelton, D. B., Samelson, R. M., Schlax, M. G., & O'Neill, L. W. (2015). Satellite observations of mesoscale eddy-induced Ekman pumping. *Journal of Physical Oceanography*, *45*(1), 104–132. https://doi.org/10.1175/JPO-D-14-0032.1

Gill, A. E. (Ed.), (1982). *Atmosphere-ocean dynamics* (Vol. 30). Academic Press.

Haller, G., & Beron-Vera, F. J. (2013). Coherent Lagrangian vortices: The black holes of turbulence. *Journal of Fluid Mechanics*, *731*, R4. https://doi.org/10.1017/jfm.2013.391

Hamilton, P., Fargion, G. S., & Biggs, D. C. (1999). Loop Current eddy paths in the western Gulf of Mexico. *Journal of Physical Oceanography*, *29*(6), 1180–1207. https://doi.org/10.1175/1520-0485(1999)029⟨1180:LCEPIT⟩2.0.CO;2

Hamilton, P., Leben, R., Bower, A., Furey, H., & Pérez-Brunius, P. (2018). Hydrography of the Gulf of Mexico using autonomous floats. *Journal of Physical Oceanography*, *48*(4), 773–794. https://doi.org/10.1175/JPO-D-17-0205.1

Hersbach, H., Bell, B., Berrisford, P., Hirahara, S., Horányi, A., Muñoz-Sabater, J., et al. (2020). The ERA5 global reanalysis. *Quarterly Journal of the Royal Meteorological Society*, *146*(730), 1999–2049. https://doi.org/10.1002/qj.3803

Holliday, D., & McIntyre, M. E. (1981). On potential energy density in an incompressible, stratified fluid. *Journal of Fluid Mechanics*, *107*(-1), 221–225. https://doi.org/10.1017/S0022112081001742

Jaimes, B., Shay, L. K., & Brewster, J. K. (2016). Observed air-sea interactions in tropical cyclone Isaac over Loop Current mesoscale eddy features. *Dynamics of Atmospheres and Oceans*, *76*, 306–324. https://doi.org/10.1016/j.dynatmoce.2016.03.001

Jouanno, J., Ochoa, J., Pallàs-Sanz, E., Sheinbaum, J., Andrade-Canto, F., Candela, J., & Molines, J.-M. (2016). Loop Current Frontal Eddies: Formation along the campeche bank and impact of coastally trapped waves. *Journal of Physical Oceanography*, *46*(11), 3339–3363. https://doi.org/10.1175/JPO-D-16-0052.1

Joyce, T. M., Toole, J. M., Klein, P., & Thomas, L. N. (2013). A near-inertial mode observed within a Gulf Stream warm-core ring. *Journal of Geophysical Research: Oceans*, *118*(4), 1797–1806. https://doi.org/10.1002/jgrc.20141

Kantha, L., Choi, J.-K., Schaudt, K. J., & Cooper, C. K. (2005). A regional data-assimilative model for operational use in the Gulf of Mexico. *Washington DC American Geophysical Union Geophysical Monograph Series*, *161*, 165–180. https://doi.org/10.1029/161GM14

Kunze, E. (1986). The mean and near-inertial velocity fields in a warm-core ring. *Journal of Physical Oceanography*, *16*(8), 1444–1461. https://doi.org/10.1175/1520-0485(1986)016⟨1444:TMANIV⟩2.0.CO;2

Larrañaga, M., Renault, L., & Jouanno, J. (2022). Partial control of the Gulf of Mexico dynamics by the current feedback to the atmosphere. *Journal of Physical Oceanography*, *52*(10), 2515–2530. https://doi.org/10.1175/JPO-D-21-0271.1

Leben, R. R. (2005). Altimeter-derived loop current metrics. *Washington DC American Geophysical Union Geophysical Monograph Series*, *161*, 181–201. https://doi.org/10.1029/161GM15

Le Hénaff, M., Kourafalou, V. H., Androulidakis, Y., Ntaganou, N., & Kang, H. (2023). Influence of the Caribbean Sea eddy field on loop current predictions. *Frontiers in Marine Science*, *10*, 1129402. https://doi.org/10.3389/fmars.2023.1129402

Lipphardt, B. L., Poje, A. C., Kirwan, A. D., Kantha, L., & Zweng, M. (2008). Death of three loop current rings. *Journal of Marine Research*, *66*(1), 25–60. https://doi.org/10.1357/002224008784815748

Lugo-Fernández, A., Leben, R. R., & Hall, C. A. (2016). Kinematic metrics of the Loop Current in the Gulf of Mexico from satellite altimetry. *Dynamics of Atmospheres and Oceans*, *76*, 268–282. https://doi.org/10.1016/j.dynatmoce.2016.01.002

Mariotti, A., Legras, B., & Dritschel, D. G. (1994). Vortex stripping and the erosion of coherent structures in two-dimensional flows. *Physics of Fluids*, *6*(12), 3954–3962. https://doi.org/10.1063/1.868385

Marsh, R., Hazeleger, W., Yool, A., & Rohling, E. J. (2007). Stability of the thermohaline circulation under millennial CO_2 forcing and two alternative controls on Atlantic salinity. *Geophysical Research Letters*, *34*(3), L03605. https://doi.org/10.1029/2006GL027815

Meunier, T., Ménesguen, C., Schopp, R., & Le Gentil, S. (2015). Tracer stirring around a meddy: The formation of layering. *Journal of Physical Oceanography*, *45*(2), 407–423. https://doi.org/10.1175/jpo-d-14-0061.1

Meunier, T., Pérez-Brunius, P., & Bower, A. (2022). Reconstructing the three-dimensional structure of Loop Current Rings from satellite altimetry and in situ data using the gravest empirical modes method. *Remote Sensing*, *14*(17), 4174. https://doi.org/10.3390/rs14174174

Meunier, T., Sheinbaum, J., Pallàs-Sanz, E., Tenreiro, M., Ochoa, J., Ruiz-Angulo, A., et al. (2020). Heat content anomaly and decay of warm-core rings. *the Case of the Gulf of Mexico*, *47*(3), e85600. https://doi.org/10.1029/2019GL085600

Middleton, L., Fine, E. C., MacKinnon, J. A., Alford, M. H., & Taylor, J. R. (2021). Estimating Dissipation rates associated with double diffusion. *Geophysical Research Letters*, *48*(15), e92779. https://doi.org/10.1029/2021GL092779

Molina, M. J., Timmer, R. P., & Allen, J. T. (2016). Importance of the Gulf of Mexico as a climate driver for U.S. severe thunderstorm activity. *Geophysical Research Letters*, *43*(23), 12295–12304. https://doi.org/10.1002/2016GL071603

Oey, L. Y., Lee, H. C., & Schmitz, W. J. (2003). Effects of winds and Caribbean eddies on the frequency of Loop Current eddy shedding: A numerical model study. *Journal of Geophysical Research*, *108*(C10), 3324. https://doi.org/10.1029/2002JC001698

Pérez, J. G. C., Pallàs-Sanz, E., Tenreiro, M., Meunier, T., Jouanno, J., & Ruiz-Angulo, A. (2022). Overturning instabilities across a warm core ring from glider observations. *Journal of Geophysical Research: Oceans*, *127*(4), e2021JC017527. https://doi.org/10.1029/2021JC017527

Plagge, A. M., Vandemark, D., & Chapron, B. (2012). Examining the impact of surface Currents on satellite scatterometer and altimeter ocean winds. *Journal of Atmospheric and Oceanic Technology*, *29*(12), 1776–1793. https://doi.org/10.1175/JTECH-D-12-00017.1

Polzin, K. L. (2008). Mesoscale eddy-internal wave coupling. Part I: Symmetry, wave capture, and results from the mid-ocean dynamics experiment. *Journal of Physical Oceanography*, *38*(11), 2556–2574. https://doi.org/10.1175/2008JPO3666.1

Renault, L., Marchesiello, P., Masson, S., & McWilliams, J. C. (2019). Remarkable control of western boundary currents by eddy killing. *A Mechanical Air-Sea Coupling Process*, *46*(5), 2743–2751. https://doi.org/10.1029/2018GL081211

Renault, L., McWilliams, J. C., & Penven, P. (2017). Modulation of the Agulhas current retroflection and leakage by oceanic current interaction with the atmosphere in coupled simulations. *Journal of Physical Oceanography*, *47*(8), 2077–2100. https://doi.org/10.1175/JPO-D-16-0168.1

Renault, L., Molemaker, M. J., Gula, J., Masson, S., & McWilliams, J. C. (2016). Control and stabilization of the Gulf Stream by oceanic current interaction with the atmosphere. *Journal of Physical Oceanography*, *46*(11), 3439–3453. https://doi.org/10.1175/JPO-D-16-0115.1

Renault, L., Molemaker, M. J., McWilliams, J. C., Shchepetkin, A. F., Lemarié, F., Chelton, D., et al. (2016). Modulation of wind work by oceanic current interaction with the atmosphere. *Journal of Physical Oceanography*, *46*(6), 1685–1704. https://doi.org/10.1175/JPO-D-15-0232.1

Romanou, A., Chassignet, E. P., & Sturges, W. (2004). Gulf of Mexico circulation within a high-resolution numerical simulation of the North Atlantic Ocean. *Journal of Geophysical Research*, *109*(C1), C01003. https://doi.org/10.1029/2003JC001770

Scatterometer Wind Fields (2023). Global ocean monthly mean sea surface wind and stress from scatterometer and model [scatterometer wind dataset]. Copernicus. https://doi.org/10.48670/moi-00181

Schmitt, R. W., Lueck, R. G., & Joyce, T. M. (1986). Fine- and microstructure at the edge of a warm-core ring. *Deep-Sea Research A*, *33*(11–12), 1665–1689. https://doi.org/10.1016/0198-0149(86)90073-7

Shay, L. K., Goni, G. J., & Black, P. G. (2000). Effects of a warm oceanic feature on hurricane opal. *Monthly Weather Review*, *128*(5), 1366–1383. https://doi.org/10.1175/1520-0493(2000)128<1366:eoawof>2.0.co;2

Stern, M. E. (1965). Interaction of a uniform wind stress with a geostrophic vortex. *Deep-Sea Research A*, *12*(3), 355–367. https://doi.org/10.1016/0011-7471(65)90007-0

Sturges, W., Evans, J. C., Welsh, S., & Holland, W. (1993). Separation of warm-core rings in the Gulf of Mexico. *Journal of Physical Oceanography*, *23*(2), 250–268. https://doi.org/10.1175/1520-0485(1993)023⟨0250:SOWCRI⟩2.0.CO;2

Sun, C., & Watts, D. R. (2001). A circumpolar gravest empirical mode for the. *Southern Ocean hydrography*, *106*(C2), 2833–2855. https://doi.org/10.1029/2000JC900112

Tedesco, P., Gula, J., Ménesguen, C., Penven, P., & Krug, M. (2019). Generation of submesoscale frontal eddies in the Agulhas Current. *Journal of Geophysical Research: Oceans*, *124*(11), 7606–7625. https://doi.org/10.1029/2019JC015229

Vidal, V. M. V., Vidal, F. V., Hernández, A. F., Meza, E., & Zambrano, L. (1994). Winter water mass distributions in the western Gulf of Mexico affected by a colliding anticyclonic ring. *Journal of Oceanography*, *50*(5), 559–588. https://doi.org/10.1007/bf02235424

Vukovich, F. M. (2007). Climatology of ocean features in the Gulf of Mexico using satellite remote sensing data. *Journal of Physical Oceanography*, *37*(3), 689–707. https://doi.org/10.1175/JPO2989.1

Watts, D. R., Sun, C., & Rintoul, S. (2001). A two-dimensional gravest empirical mode determined from hydrographic observations in the subantarctic front. *Journal of Physical Oceanography*, *31*(8), 2186–2209. https://doi.org/10.1175/1520-0485(2001)031⟨2186:ATDGEM⟩2.0.CO;2

Wilder, T., Zhai, X., Munday, D., & Joshi, M. (2022). The response of a baroclinic anticyclonic eddy to relative wind stress forcing. *Journal of Physical Oceanography*, *52*(9), 2129–2142. https://doi.org/10.1175/jpo-d-22-0044.1

Winters, K. B., Lombard, P. N., Riley, J. J., & D'Asaro, E. A. (1995). Available potential energy and mixing in density-stratified fluids. *Journal of Fluid Mechanics*, *289*, 115–128. https://doi.org/10.1017/S002211209500125X